Chemical Physics Impact 8 (2024) 100594

Contents lists available at ScienceDirect

Chemical Physics Impact

journal homepage: www.sciencedirect.com/journal/chemical-physics-impact

Full Length Article

Optoelectronic and mechanical properties of gallium arsenide alloys: Based on density functional theory

A.A. Adewale [a,i,*], A.A. Yahaya [b,c], L.O. Agbolade [d,e], O.K. Yusuff [f], S.O. Azeez [a,g], K.K. Babalola [a,g], K.O. Suleman [h], Y.K. Sanusi [a,i], A. Chik [j,k,*]

[a] Department of Pure and Applied Physics, Ladoke Akintola University of Technology, Ogbomoso, Nigeria
[b] Department of Physics and Materials Science, Kwara State University, Malete, Nigeria
[c] Department of Physics, Kebbi State University of Science and Technology, Aliero, Nigeria
[d] Institute of Nano Electronic Engineering, Universiti Malaysia Perlis, 01000, Perlis, Kangar Malaysia
[e] Department of Physics, University of Central Florida, Orlando, FL 32816, USA
[f] Department of Chemistry, University of Ilorin, Ilorin, Nigeria
[g] Department of Physical and Chemical Sciences, Federal University of Health Sciences, Ila- Orangun, Nigeria
[h] Department of Physics, Nigeria Maritime University, Okerenkoko, Warri, Nigeria
[i] Nanotechnology Research Group (NANO+), Ladoke Akintola University of Technology, Ogbomoso, Nigeria
[j] Center of Excellence Geopolymer and Green Technology (CEGeoGTech), School of Materials Engineering, Universiti Malaysia Perlis (UniMAP), 02600, Jejawi, Arau, Perlis, Malaysia
[k] Faculty of Chemical Engineering, Materials Engineering, Universiti Malaysia Perlis (UniMAP), Taman Muhibbah, 02600, Jejawi, Arau, Perlis, Malaysia

ARTICLE INFO

Keywords:
Density functional theory
Electronic property
Optical property
Mechanical property
GaAs alloys

ABSTRACT

First principles calculations based on density functional theory (DFT) were performed to investigate the structural, electronic, optical and mechanical properties of pristine GaAs compound and its alloy; $Ga_{0.75}Al_{0.25}As$, $Ga_{0.75}In_{0.25}As$, $Ga_{0.75}Sn_{0.25}As$, $Ga_{0.75}Ti_{0.25}As$. WIEN2K and Quantum expresso (QE) codes were adopted for calculations using generalized gradient approximation (GGA) in Perdew-Burke Erzenhoff (PBE) as exchange correlation function for both codes. Full potential linear augmented plane wave (FPLAPW) with the local orbital method was adopted as implement in WIEN2K code. In QE code, norm-conserving pseudopotentials were employed on a plane-wave expansion of the wave functions. Structural and electronic properties were elaborated since their result gives information about the optical and mechanical performance. Electronic band structure and optical parameters were performed using WIEN2K code. Underestimation of band gap observed from DFT calculations were corrected by using Modified Becke and Johnson (mBJ). Mechanical components were determined using QE with thermo_pw package. Lattice constant, volume, bulk modulus and other physical parameters were calculated for structural properties. Discrepancy in these parameters as observed in crystal structure is associated to difference in ionic radius of host and substituted atom. The results of band structure and density of states were calculated for electronic properties. All the studied compounds were semiconductors in nature except $Ga_{0.75}Sn_{0.25}As$ which displayed metallic character. Optical parameters including extinction coefficient, absorption coefficient, refractive index, optical conductivity, optical reflectivity and energy loss function have been computed from the dielectric function at energy range of 0 to 25 eV using the Kramers-Kronig transformations. Calculated elastic function were used to compute the mechanical properties such as anisotropic, brittle characteristics, stiffness and many others. All the results were compared with available theoretical and experimental records.

1. Introduction

Ongoing advancement in group III-V optoelectronics materials requires the investigation of semiconductor alloys with precise properties such mechanical, optical, electrical and structural properties. GaAs is a semiconductor material comprising of Gallium (Ga) and Arsenic (As) of group III and V respectively [1]. GaAs has a cubic phase of space group F-43 m [2,3] with zinc blende nature [4]. Alloys lattice- related to a given substrate offer fresh prospective to identify the required material properties and are very valuable in changing the piezoelectric field,

* Corresponding authors.
E-mail addresses: aaadewale38@lautech.edu.ng (A.A. Adewale), abdullahchik@unimap.edu.my (A. Chik).

https://doi.org/10.1016/j.chphi.2024.100594
Received 1 January 2024; Received in revised form 29 March 2024; Accepted 29 March 2024
Available online 9 April 2024

Table 1
Calculated Lattice constant, Volume, bulk modulus and bulk modulus derivative of studied compounds.

Sample	Lattice constant (Å) $a = b = c$	Volume (Å^3)	Bulk modulus (B) (GPa)	Derivative bulk modulus (B')
Pristine GaAs	5.655	180.84	75.48	4.53
Other theoretical	5.664 [29], 5.666 [30], 5.667 [31], 5.665[32]		69.711[29], 69.600 [30], 61.299[31], 69.678[32]	4.34[32]
Experimental	5.640 [33], 5.653[34]		77.000 [33], 75.500[34]	
$Ga_{0.75}Al_{0.25}As$	5.679	183.15	70.080	4.37
$Ga_{0.75}In_{0.25}As$	5.800	195.11	64.930	4.93
$Ga_{0.75}Sn_{0.25}As$	5.885	203.82	54.020	3.70
$Ga_{0.75}Tl_{0.25}As$	5.842	199.38	61.280	5.05

dislocations as well as defects of that material properties. Some of these alloys encompass extensively adopt in support of device applications include GaInNAs, GaAsP, AlGaInN and many others [5–7]. Presence of doping in materials influence photo-sensitivity of a semiconductor, always reduces the band gap and increases the absorption of semiconductor. Forbidden energy of the material can also be increased with the presence of doping, in which the photo-sensitivity reduce, changed in carrier concentration and effective mass of the material, this increases in conductivity and improved the materials transmittance [8]. Composition of electronics in materials is subjective due to the doping which enhances or buckle some properties of those materials [8].

Aluminum (Al), indium (In), tin (Sn), and thallium (Tl) along other alloys are among the promising materials due to their lattice-related properties. GaAs has energy band gap value between 1.4 eV ~ 1.5 eV [3,9], large optical absorption coefficient as well as electron mobility of 8000 cm^2/Vs at 300 K [10]. This makes it a prominent material for high-performance photo-detectors, solar cells, laser, light-emitting diodes and sensors [10–15]. With these, GaAs is one of the material preferred for fabricating good quality solar cells, sensors, light-emitting diodes and photo detectors [10].

Numerous studies have been carried out on GaAs by different researchers using various deposition methods such as screen printing techniques, sol-gel method, spray pyrolysis method, electro, molecular beam epitaxy (MBE), chemical vapor and chemical bath [16]. Also, theoretical approached in the studies of GaAs was not left out, researchers pay more attention as a result of its superb properties when it is doped with certain alloy, thereby enhancing its electronic and optical properties [17–19].

The motivation behind the present study is due to the fact that little or no research have been done in these aspects of GaAs and its doped alloys (Al, In, Sn and Tl). Hence, in this work, WIEN2k software [20] was used to calculate the ground state energy by applying Perdew-Burke-Ernzerhof (PBE) in generalized gradient approximation (GGA) exchange correlation function [21] based on density functional theory (DFT) [22]. Electronic band gap was calculated using standard DFT approach and then modified Becke Johnson (mBJ) function [23] for the improvement of underestimation that usually accompany standard DFT. Optical parameters such as conductivity, energy loss, absorption, refractive index and reflectivity were determined from dielectric function. The calculated band structures and density of states were used to evaluate the electronic properties of Gallium Arsenide and its alloys. Stability of the materials were predicted by calculating elastic constants, which were in turn used, for evaluation of mechanical parameters such as anisotropic, brittle characteristics, stiffness and many others using quantum espresso (QE).

2. Computational details

First principle calculations were performed for the investigation of structural, electronic, optical and mechanical properties of GaAs and its alloys. Pristine GaAs was chosen as control sample in order to note the influence of dopants on the model GaAs alloys. Thermo_pw package implemented in Quantum-Espresso (QE) code [24,25] was used to calculate mechanical properties. Meanwhile, WIEN2k code [20] was used for former properties calculations. This is based on full potential linearized augmented form of plane wave together with local orbital (FP-LAPW + lo) [26].

GGA-PBE were employed [21] as exchange-correlation potential. Rmt × Kmax of 8.0 was used for the expansion of the wave function at the core of interstitial region where Rmt is the minimum of the atomic sphere radii and Kmax is the plane-wave cut-off wave vector. Charge density is Fourier expansion of $G_{max} = 12$ (a.u.)$^{-1}$ while the maximum value of angular momentum $l_{max} = 10$ was used for control of partial waves expansion inside the muffin-tin spheres. The distance between core and the valence electrons are set to be −6.0 Ry and energy of convergence during scf is 10^{-4} Ry for total energy. Monkhorst-pack [27], 10 × 10 × 10 meshes was produced from 1000 optimized k-points in the irreducible wedge of the Brillouin zone.

Structural optimization was achieved through equation of state; Murnaghan's [28]. Electronic band structures were determined by means of GGA-PBE potential, but as a result of underestimated value of energy band gap which is common norms of DFT, Trans and Blaha-modified Becke–Johnson potential (TB-mBJ) [23] was used for the correction of the underestimation. For optical property calculations, very high dense of k-mesh 25 × 25 × 50 in the full BZ integration was adopted in order to achieved excellent result.

We calculated the optical properties via the real $\varepsilon_1(\omega)$and imaginary $\varepsilon_2(\omega)$ components of the dielectric function $\varepsilon(\omega)$. From Kramers-Kronig transformation, $\varepsilon_2(\omega)$ can be calculated [29,30];

$$\varepsilon_2(\omega) = \frac{Ve^2}{2\pi\hbar m^2\omega^2}\int d^3k\sum_m \left|\left\langle \vec{k}\,n|P|\vec{k}\,n'\right\rangle\right|^2 f_n^{\vec{k}}\left(1-f_n^{\vec{k}'}\right)\delta\left(E_n^{\vec{k}} - E_{n'}^{\vec{k}} - \hbar\omega\right) \tag{1}$$

where ω, P, e, and $\vec{k}$ denotes the angular frequency of the electromagnetic wave, momentum, electron charge, and wave vector, in that order. $f_n^{\vec{k}}$ and $\delta(E_n^{\vec{k}} - E_n^{\vec{k}} - \hbar\omega)$ are the Fermi distribution and its Dirac functions, respectively. While, n and n' means original and final states of electron in a system. The $\varepsilon_1(\omega)$ can be determined from the $\varepsilon_2(\omega)$ using the Kramers-Kronig relations;

$$\varepsilon_1(\omega) = 1 + \frac{2}{\pi}A\int_0^\infty \frac{\omega'\varepsilon_2(\omega')}{\omega'^2 - \omega^2}d\omega' \tag{2}$$

where, A represent the integral value.

The dielectric function $\varepsilon(\omega)$ for optical properties of materials is defined by the expression;

$$\varepsilon(\omega) = \varepsilon_1(\omega) + i\varepsilon_2(\omega) \tag{3}$$

The dielectric function is the basic optical parameter which other parameters depend [31,32];

$$\text{Absorptioncoefficient}\quad A(\omega) = \frac{\sqrt{2}\omega}{c}\left[\sqrt{\varepsilon_1{}^2(\omega) + \varepsilon_2{}^2(\omega)} - \varepsilon_1(\omega)\right]^{1/2} \tag{4}$$

where c is velocity of light.

$$\text{Opticalrefractiveindex}\quad n(\omega) = \left[\frac{\sqrt{\varepsilon_1^2(\omega) + \varepsilon_2^2(\omega)}}{2} + \frac{\varepsilon_1(\omega)}{2}\right]^{1/2} \tag{5}$$

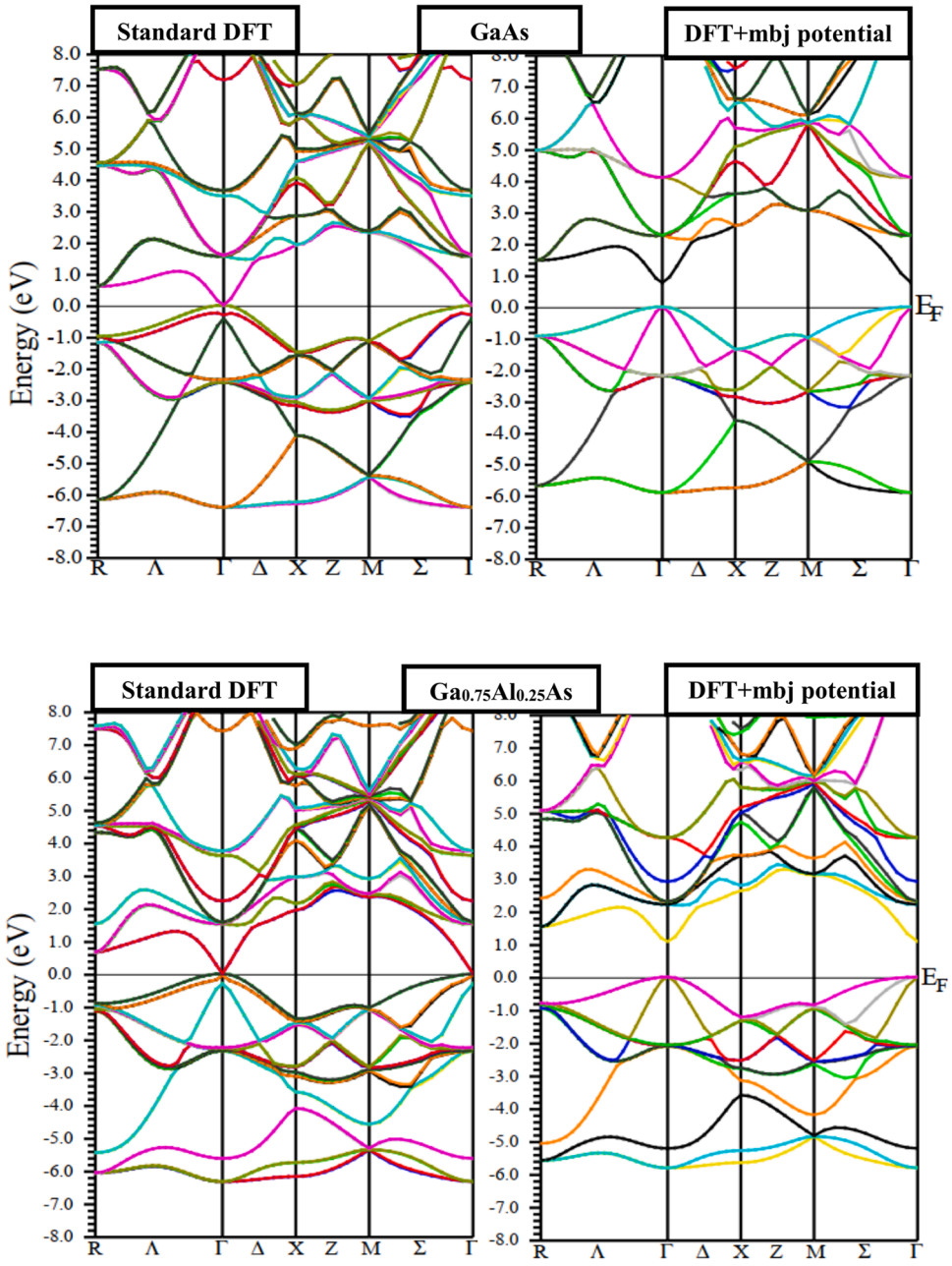

Fig. 1. Calculated band structure for pure GaAs and doped $Ga_{0.75}Al_{0.25}As$.

$$\text{Energylossfunction} \quad L(\omega) = \frac{\varepsilon_2}{(\varepsilon_2(\omega)^2 + \varepsilon_1(\omega)^2)} \tag{6}$$

$$\text{Opticalconductivity} \quad \sigma(\omega) = -i\frac{\omega}{4\pi}|\varepsilon(\omega) - 1| \tag{7}$$

and

$$\text{Extinctioncoefficient} \quad k(\omega) = \left[\frac{\sqrt{\varepsilon_1^2(\omega) + \varepsilon_2^2(\omega)}}{2} - \frac{\varepsilon_1(\omega)}{2}\right]^{1/2} \tag{8}$$

3. Results and discussion

3.1. Crystal structure

GaAs cubic crystal structure and their alloys ($Ga_{0.75}Al_{0.25}As$, $Ga_{0.75}In_{0.25}As$, $Ga_{0.75}Sn_{0.25}As$ and $Ga_{0.75}Tl_{0.25}As$) were studied. Using Murnaghan's equation of state [28], samples were optimized by fitting total energy against volume;

$$E_{tot}(V) = E_0 + \frac{B_0 V}{B_0'(B_0'-1)}\left\{B_0'\left(1 - \frac{V_0}{V}\right) + \left(\frac{V_0}{V}\right)^{B_0'} - 1\right\} \tag{9}$$

Where E(V) is the total energy with the volume, V_0 is the equilibrium volume at minimum E_{tot}, while B_0 and B_0' is bulk modulus and its derivative respectively. The calculated optimized lattice parameter (a, b and c), volume (V), bulk modulus (B) and bulk modulus derivative (B_0') are shown in Table 1. Our calculated lattice constant for pristine GaAs is 5.655 Å and it is in good agreement with several theoretical [32–36] and experimental work [37,38] as presented in Table 1. Space group of pristine GaAs is F-43 m (216) [3], the face centre cubic crystal structure, which later change to P-43 m (215) as predicted for all model alloys using WIEN2k code. This can be due to variation in the atomic mass of dopant and replaced Ga atom.

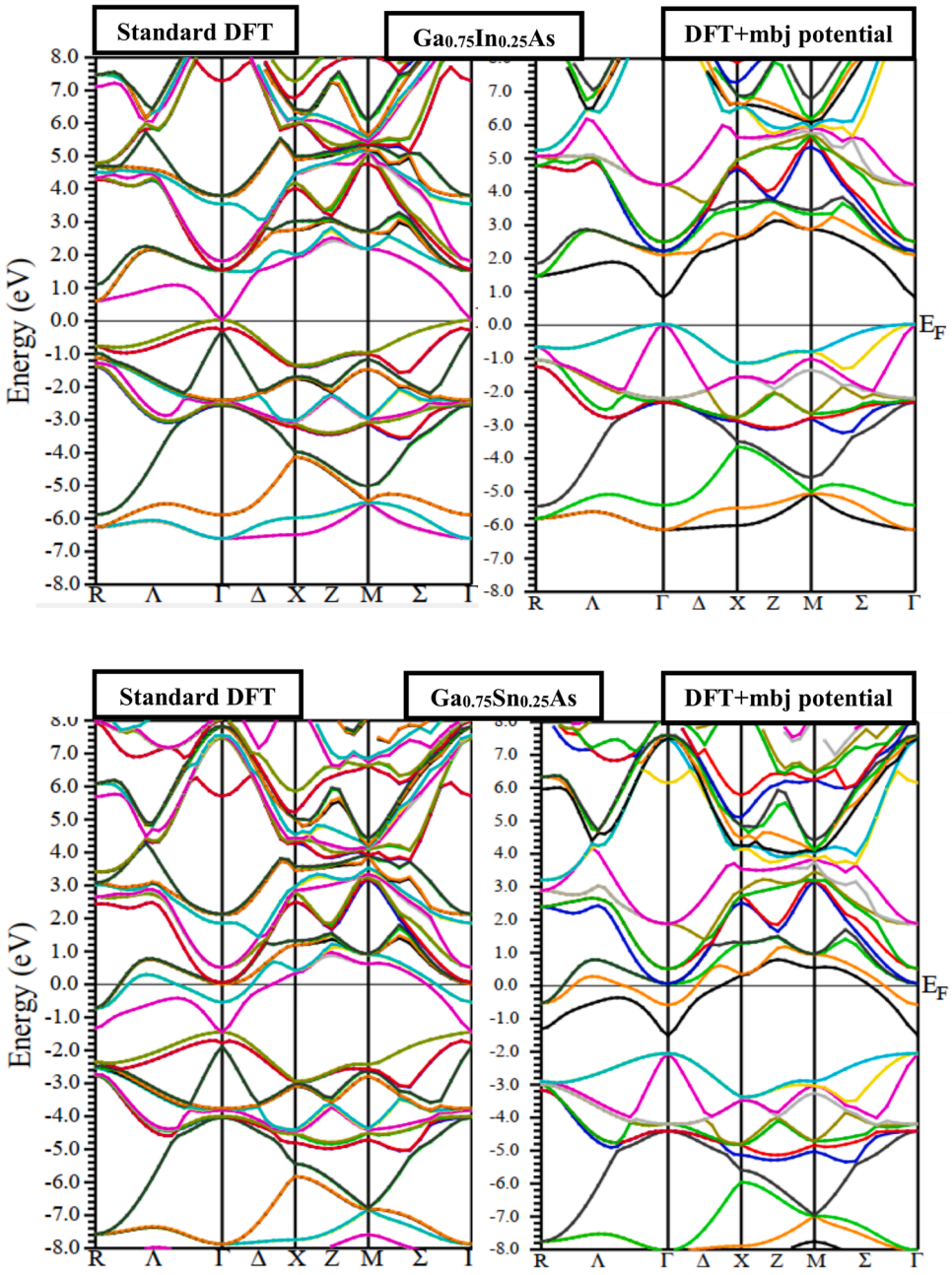

Fig. 2. Calculated band structure for $Ga_{0.75}In_{0.25}As$ and doped $Ga_{0.75}Sn_{0.25}As$.

3.2. *Electronic properties*

The electronic band structure and density of states (DOS) were determined to reveal more facts about the materials electronic properties. These are important features in modeling of electronic devices. The electronic band structure of all the studied samples were calculated along high symmetry path R –Γ –X – M – Γ of the Brillouin zone as presented in Figs. 1–3. The Fermi energy level (E_f) is fixed to zero energy. The conduction and valence band (CB and VB) are at Γ– point direction of high symmetry which indicate direct band gap and semiconductor nature of the materials. With standard DFT, the band gap of GaAs was found to be 0.2857 eV, a clear underestimation when compared to experiment [39]. This is the general trend of simulation work [40,41]. The present result is similar to the one reported by Ahmed et al., in their work, Ab initio study of structural and electronic properties of III-arsenide binary compounds [42]. The result of calculated band structure with DFT + TB-mbJ potential is in excellent agreement when compared to other theoretical work [40,42] but there is slight difference when compared to experimental work [39] as presented in Table 2. In Figs. 1–3, it was observed that the presence of impurities (Al, In, Sn and Tl) alter the present feature of GaAs alloys band gap. With the exception of Sn dopant which reveal metallic nature with zero of band gap, all the doped samples are still depicting semiconductor feature when calculated with TB-mBJ potential. The new band gaps with DFT+TB-mBJ were presented in Table 2.

To obtain useful information of a material with regards to electron movement from one orbit to another i.e. the conduction band orbit and valence band orbit within the same period of time, density of state is used. Band structure and density of state was used to control the electronic orbital movement from one energy level to another. Doping of a material change its density of state by depreciating the electronic performance of the materials, i.e. increasing or decreasing the optical performance of the materials [43].

In order to reveal the contribution of each atomic orbital in the

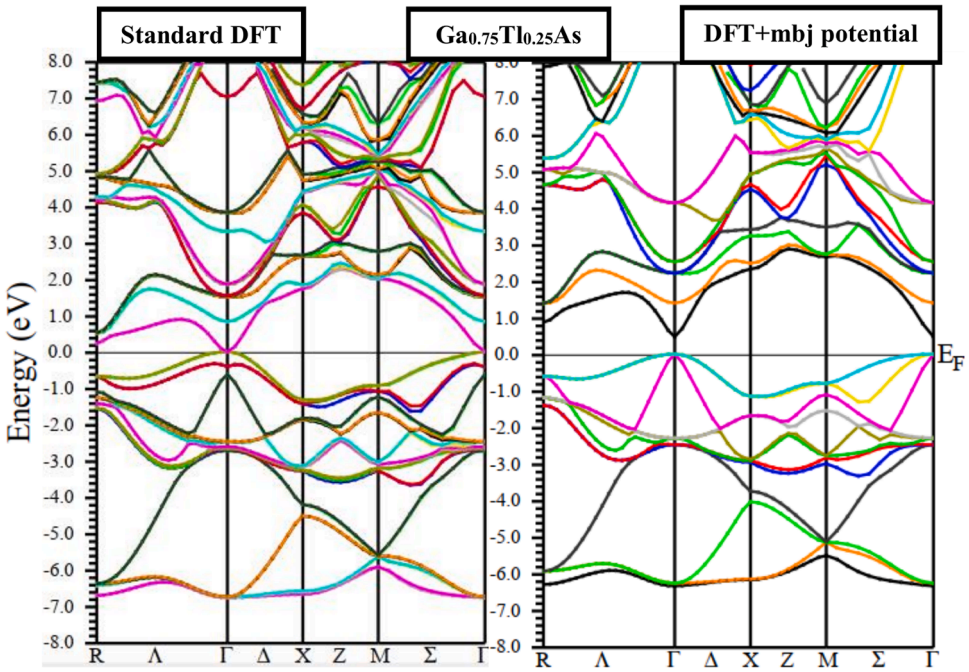

Fig. 3. Calculated band structure for $Ga_{0.75}Tl_{0.25}As$.

Table 2
Band gap of studied compounds using DFT and DFT+mbj where compared to other theoretical as well as experimental.

Sample	DFT (eV)	DFT+mbj (eV)	Others (eV)
Pristine GaAs	0.2857	1.6190	
Other theoretical	0.341[36]	1.560[36], 1.640[36]	0.28[37,42] 1.50[38]
Experimental			1.520[35]
$Ga_{0.75}Al_{0.25}As$	0.5476	1.7619	
$Ga_{0.75}In_{0.25}As$	–	1.000	
$Ga_{0.75}Sn_{0.25}As$	–	–	
$Ga_{0.75}Tl_{0.25}As$	–	0.619	

building of band structure as well as orbital contributions to the changing of band gap, we calculated the partial density of state as displayed in Figs. 4–8. The Fermi energy level, which is set at zero energy was represented by vertical dotted line. Symmetric spin in both channels of plots were observed for all sample, an indication that the materials are non-magnetic in character even with the presence of dopant. From Figs. 4–8, it was observed that the semiconductor nature of materials were from As-4p orbital at both electronic band; valence and conduction, with little contribution from Ga-4p and As-3d orbitals, except $Ga_{0.75}Sn_{0.25}As$ that is metallic in nature as a result of shifting in Fermi energy level. Our result is consistence with the band structure calculation reported earlier.

3.3. Optical properties

In the process of designing optoelectronic devices, precise understanding of certain optical parameters of materials are needed. The optical properties were determined using electronic transition as employed by time-dependent perturbations of the total electronic state [32]. This shows that investigations of optical properties are directly linked to the energy band gap of materials. The calculated optical parameters for all the studied compounds were in the energy range 0 – 25 eV. Polarizations of only x-axis direction were considered since x- and z-axis are symmetric for cubic crystal system. Complex dielectric function was originally evaluated since other parameters depend on it and this also influences the incident electromagnetic waves on materials.

3.3.1. Dielectric function

The dielectric function pronounces sensitivity of a semiconductor to electromagnetic carried via photons and electrons [44]. The real and imaginary parts of complex dielectric function of GaAs and $Ga_{0.75}A_{0.25}As$ (A=Al, In, Sn and Tl) were presented in Figs. 3 and 4. In the real part of dielectric, the static dielectric $\varepsilon_1(0)$ is the zero energy of the dielectric. The $\varepsilon_1(0)$ of GaAs, $Ga_{0.75}Al_{0.25}As$, $Ga_{0.75}In_{0.25}As$, $Ga_{0.75}Sn_{0.25}As$, and $Ga_{0.75}Tl_{0.25}As$ were 18.2, 15.5, 17.2, 29.5 and 20.4 respectively. These differences in performance is related to the changes in their electronic band structures; in particular, the metallic material gives high static dielectric and material with wide band gap in the study is the least. This shows that electronic band gap value is inversely proportional to static dielectric constant of a material as it is inversely proportional to the wavelength of the electromagnetic wave [45]. The photon energy of visible light ranges from 2 to 2.75 eV [45,46]. Semiconductor sample depict concave feature at visible range while only metallic shows the convex with very high value of dielectric constant compared to formal. In pristine GaAs, 12.74 were obtained for dielectric constant $\varepsilon_1(\omega)$ at photon energy of 2.00 eV which is in the same range 12 - 12.9 reported in Ref. [47,48]. It was observed that as from 10 eV of photon energy, the dielectric constant of all the studied sample are uniform and approximately the same, which is the same trends for real part of dielectric constant in other study [49].

Imaginary part $\varepsilon_2(\omega)$ of the dielectric determines the light absorption characteristics of the material. Two prominent sharp peaks were revealed in the imaginary dielectric plots of all compounds. In metallic character $Ga_{0.75}Sn_{0.25}As$, first sharp peak was observed below visible light region while the first peaks for the studied semiconductors falls within the visible region. This shows strong absorption of metallic over semiconductor materials, making it more relevant for energy harvesting devices. The observed peaks at the ultraviolet region were higher than those of the visible region. The static imaginary dielectric constant in the studied compounds decreases as band gap increases. This is related to the shortest inter-band transitions between maximum of VB and minimum of CB. Normally, dielectric constant of materials increases as a

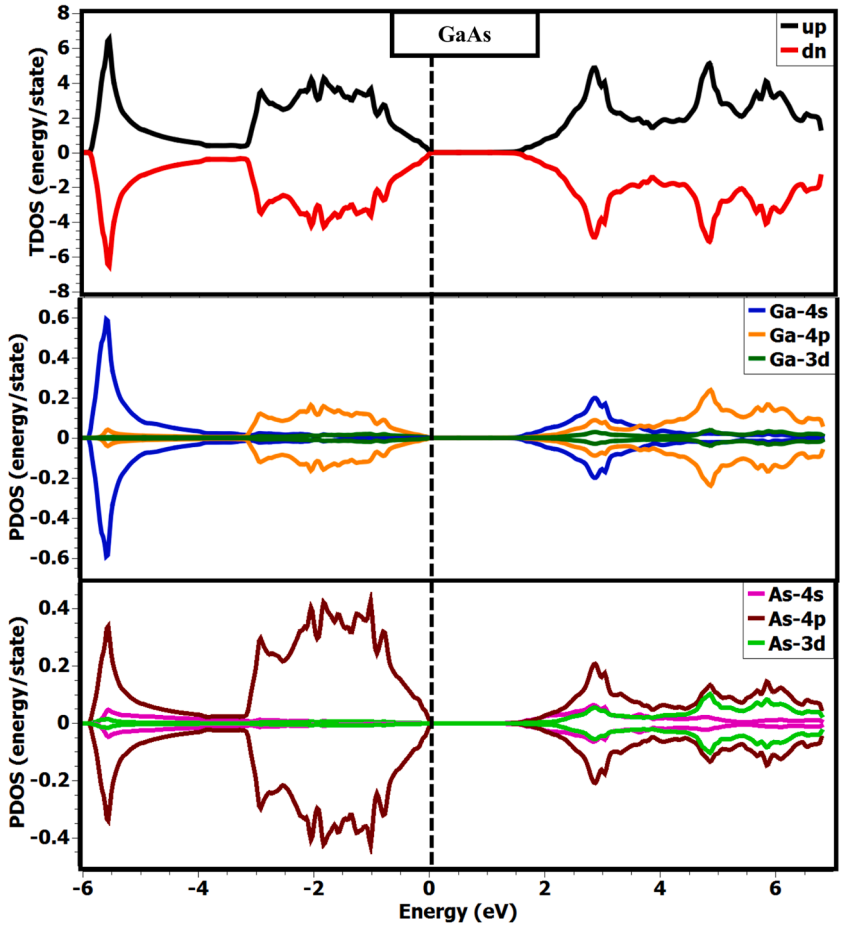

Fig. 4. Total and partial density of states for GaAs.

result of their molecules polarization. Besides, both low and high values of dielectric constant ε(ω) are noteworthy and essential in electronic engineering.

Fig. 9

3.3.2. *Absorption coefficient*

Absorption Coefficient is one of the properties of an optoelectronic devices which is defined as the light engrossed per unit length of the material [32]. When optoelectronic material absorbs light, it leads to the movement of electrons from one band level to another. Good absorber material absorbs all electromagnetic radiation incident on it, leading to the total escape of unexcited electrons through the radiation. If material's photon energy is less than the band energy, light will not be absorbed by the material. Therefore, for the material to absorb light, photon energy must be greater than the band energy. Fig. 10a shows that pristine GaAs and its alloys possess zero absorption at 0 eV, with a significant increase in absorption value at 1.2 eV. The absorption reaches its Peak value of 170×10^4 cm^{-1} at 6 eV, which was the highest of the studied samples. The lowest value was observed for $Ga_{0.75}Sn_{0.25}As$. Generally, the absorption values started decreasing from photon energy of 6 eV until it reaches a uniform of 20×10^4 cm^{-1} at 21 eV. In this study absorption peaks are in the range of ultraviolet region with approximately 7 eV for the pristine GaAs and its alloys. $Ga_{0.75}Al_{0.25}As$ has strongest absorption in ultraviolet zone when compared to other studied samples which makes it more suitable for optoelectronic devices application.

3.3.3. *Refractive index*

Refractive index (n) is one of the good factor or character of light absorbing material, as it gives information on how light will behave within the material [32]. Refractive index of pristine GaAs and doped GaAs are displayed in Fig. 10b, where at static refractive index (0 eV), n at the range of 3.9 to 5.4 ω were observed. The static refractive index is a useful concept for understanding the properties of materials in the limit of low photon energies. From the Fig. 10b, $Ga_{0.75}Sn_{0.25}As$ has the highest value of refractive index at 0 eV (5.4 ω) depicted the distinct nature of material, a metallic. Metallic compound with free transport of electrons have large values of refractive index because of its ability to move freely. Meanwhile, $Ga_{0.75}Tl_{0.25}As$ has the highest 'n' 4.7 ω at 2.0 eV the visible region. This is in correlation with the energy band gap result in Table 2, that is the narrowly the band gap the higher the refraction index of the material. The refractive index is normally used to regulate the transparency of materials. From our results, semiconductors samples have conspicuous band gaps in the visible range and are fitting with Penn's model, $\varepsilon_1(0) = 1 + (h\omega p/Eg)^2$ [50]. This will make them suitable for optoelectronic devices.

3.3.4. *Optical conductivity*

The absorption of incident energy by a material resulted in the creation of free electrons which can be reveals by the conductivity (σ) [32], in this study optical conductivity of GaAs and its alloys were presented in Fig. 10c. There is high value of optical conductivity at ultraviolet region which is correlation with the earlier report on absorptivity's of the materials. We observed peak conductivity between 0 and 1 eV in metallic compounds. Meanwhile, pristine GaAs and its modelled alloyed compound gives better optical conductivity at ultraviolet region. Changing in optical conductivity over the energy range of study has the same trend with variation in refractive index, which confirmed the relations between the two terms in Eq. (7). The inter band changes of electrons from one energy level to another shows the optical

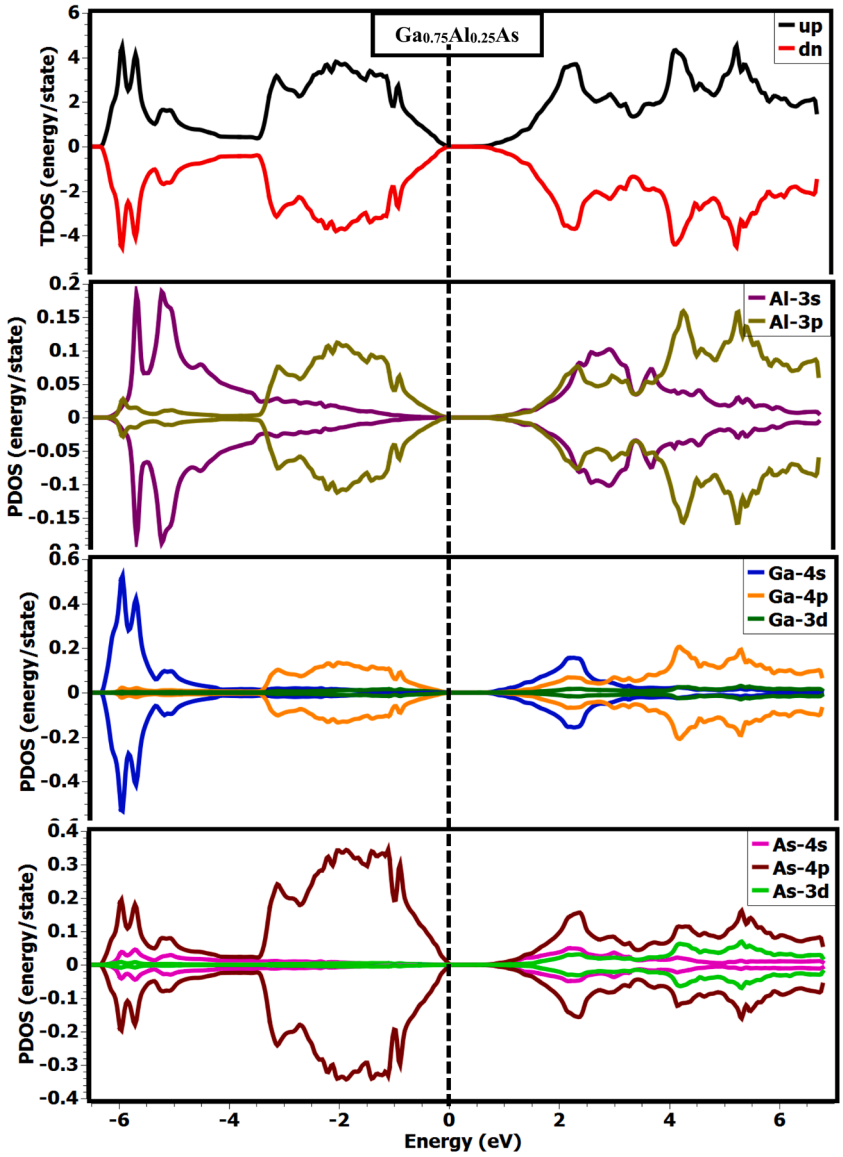

Fig. 5. Total and partial density of states for $Ga_{0.75}Al_{0.25}As$.

conductivity peaks at ultraviolet energy level [48].

3.3.5. *Optical reflectivity*

Reflectivity is one of the good properties of optoelectronics materials, as the higher the reflectivity of the material the higher the solar reflectance. In this study, the optical reflectivity was calculated from dielectric constant. The optical reflectivity against the energy was presented in Fig. 11. From the figure, it could be seen that, at 4.5 eV, both the pristine GaAs and it studied alloys has significant values of reflectivity from the region of 0.54 ω to 0.62 ω which continuous fluctuating up to 13 eV region. At 14 eV, a decreasing trend was observed, which becomes uniform at about 25 eV and continues moving with a reflectivity of 0.2 ω. Pristine GaAs has a high reflectivity at 0.62 ω in 4.5 eV while the lowest reflectivity occur in $Ga_{0.75}Sn_{0.25}As$ which recorded the lowest reflectivity value of 0.56 ω at 4.8 eV. Anti-reflection industry uses materials with lower reflectivity of less than 1 in all the range of energy [48,51].

3.3.6. *Extinction coefficient*

The extinction coefficient reveals the capacity of a material to retain light incident on it, which is one of the properties of optoelectronics materials [52]. In this study, extinction coefficient of pristine GaAs and its studied alloys is shown in Fig. 11. From the plots, maximum value of extinction coefficient, depicted by sharp peaks was observed in the energy range, which falls in ultraviolet region. For pristine GaAs and GaAs doped with its alloys, the lower energies have sharp peaks from the plots while there is decrease in absorption at high energy values. The figure also showed that peak extinction coefficient value of 4.6 ω at 2 eV was obtained for $Ga_{0.75}In_{0.25}As$, followed by pristine GaAs with 4.00 ω at 4.9 eV. The sample material with least extinction coefficients value is $Ga_{0.75}Tl_{0.25}As$, with 3.2 ω at 4.9 eV. A gradual decrease in the peaks was observed to begin after 5.0 eV.

3.3.7. *Energy loss function*

Categories of nanostructure and microstructures can be obtained using energy loss spectroscopy (EELS). EELS can be used to study elastically scattered and non-scattered electrons, it also helps in knowing the atomic number which can be strike by the beam [53,54]. When electrons of electromagnetic light pass through the material, there is loss of energy because of the fast movements of electrons. This can only be obtained using the energy loss function L(ω) process. One of the fast density oscillations uses in metals and plasmas for their conductivity is plasma

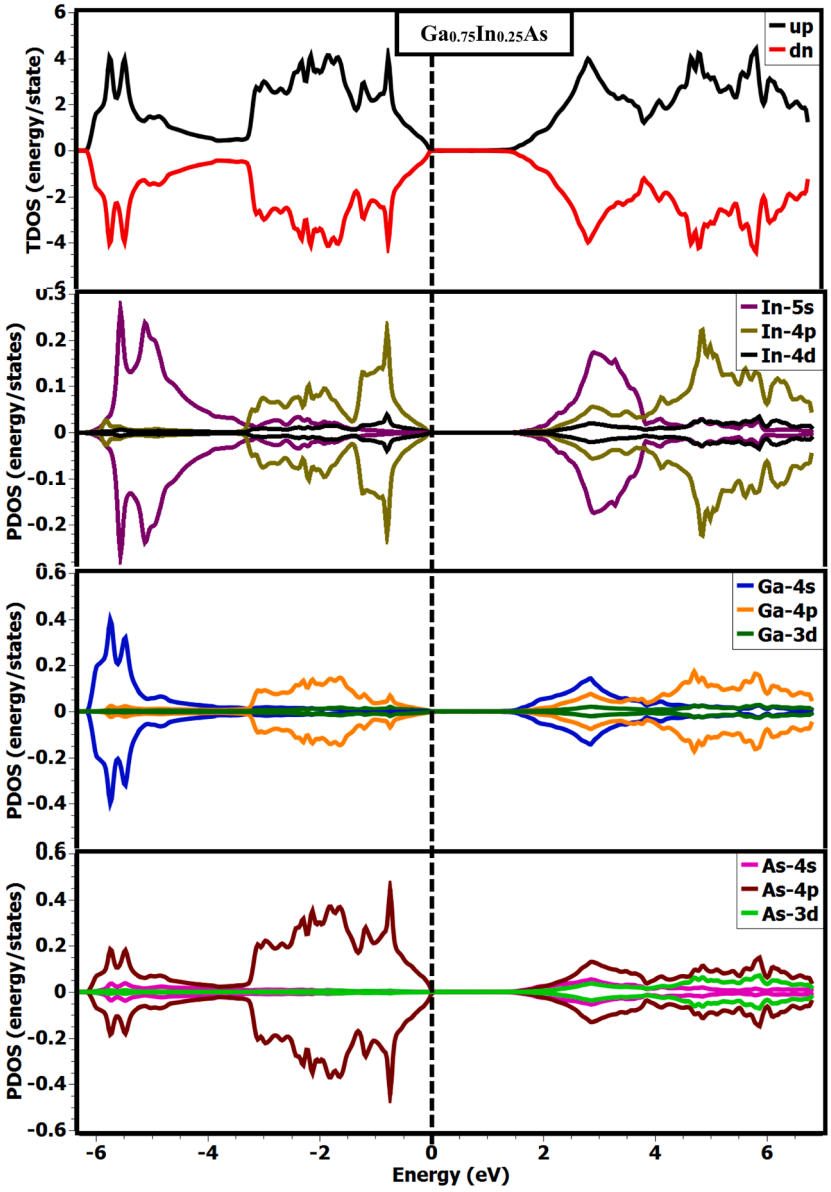

Fig. 6. Total and partial density of states for $Ga_{0.75}In_{0.25}As$.

oscillations. Plasma oscillation use in either metals or plasma in the ultraviolet zone always unfasten with the lattice area because of the fast movements of electrons [55,56]. Calculated energy loss functions were determined from real and imaginary dielectric as presented in Fig. 11. High peak intensity of 4.9 ω at 17.5 eV was observed for pristine GaAs with $Ga_{0.75}Sn_{0.25}As$ recording the second lowest value of 4.4 ω at 15.5 eV. The figure of energy loss function shows that there is clear scattering as all the studied compound were studied with zero energy loss at visible range [32]. Electron loss energy is caused by the inelastic scattering of electrons due to the incident light that falls on it, which led to the high peaks by the loss function of compounds. GaAs and $Ga_{0.75}Al_{0.25}As$ compound have high values of intensity peaks which satisfy nature of good semiconductor materials.

3.4. Mechanical properties

Determining the material's mechanical and elastic properties is essential during the manufacturing process [57,58]. Different forces can be applied when fabricating a material; therefore, it is important to understand solid forces and their atomic dynamical behaviour before applying any force to the material [57,58]. The elastic constant (C_{ij}) of the material provides clear evidence of its strength and stability. The Born-Huang theory [59] was developed by Max Born and Kun Huang and provide a thorough explanation of the mechanical stability of a material. L. Max later investigated this theory in more detail [59]. The Born-Huang elastic criteria, as proposed by Born in 1955, gave the stability requirements for cubic crystal structures as;

$$C_{11} - C_{12} > 0, C_{11} > 0, C_{44} > 0 \; and (C_{11} + 2C_{12}) > 0 \quad (10)$$

Elastic constants (C_{ij}), bulk modulus (B), and shear modulus (G) are used in Tables 3(a–e) to evaluate the stability and bonding properties of studied crystals in order to investigate their mechanical properties. To be more precise, C_{11} represents the material's resistance to strains, C_{12} represents shear stress, and C_{44} represents resistance to shear deformation. According to the Born-Huang stability principles, the elastic constant values were used to determine mechanical stability [28,60,61]. The computed elastic constants confirm the stability of the studied compounds according to the Born-Huang stability criteria. In pristine GaAs as well as doped GaAs samples, C_{11} consistently outperforms C_{12} and C_{44}, with C_{44} outperforming C_{12} in terms of values. Across all alloys

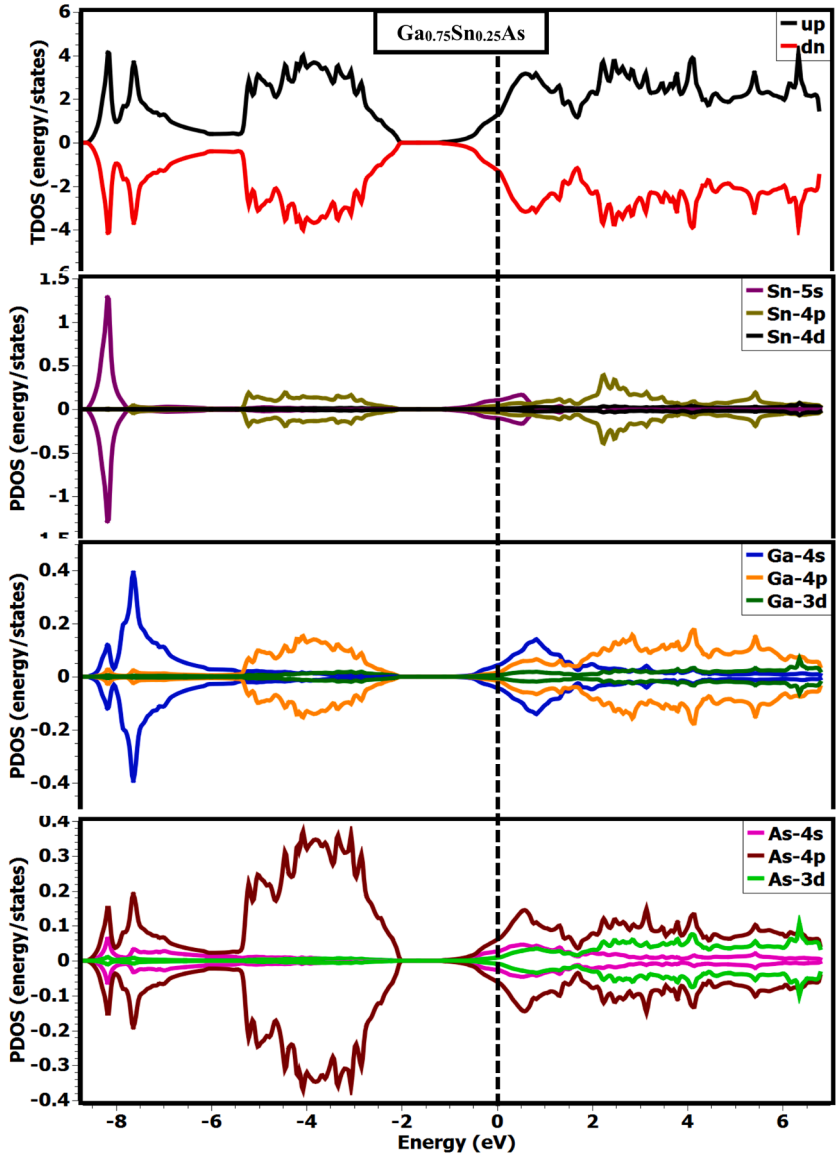

Fig. 7. Total and partial density of states for $Ga_{0.75}Sn_{0.25}As$.

under investigation, the stiffness constant shows an increasing trend with increasing pressure, according to the results. Higher bulk modulus values indicate better resistance to volume deformation and are measure of a material's resistance to compression [28,62]. The following expression was used to determine bulk moduli:

$$B = \frac{C_{11} + 2C_{12}}{3} \tag{11}$$

The strength displayed by the materials is gauged by their bulk modulus. Table 1(a) through 1(e) show that the calculated bulk modulus (B) of the studied alloys was clearly influenced by pressure. The data shows a clear relationship between higher pressure levels and higher bulk modulus values in the studied samples.

The bulk modulus of the $Ga_{0.75}Tl_{0.25}As$-doped sample is 743.0572 at 30 GPa, which is significantly higher than the value of 709.0774 recorded for the $Ga_{0.75}Al_{0.25}As$-doped sample. Notably, for all of the alloys under study, greater B values were continuously seen at the high applied pressure (30 GPa). As an example, the sample doped with $Ga_{0.75}Sn_{0.25}As$ has the lowest value of 593.3441 at 30 GPa. These results highlight the synergistic effect of doping and pressure on the bulk modulus of the studied materials.

Using Voigt's (G_v) [63] and Reuss's (G_r) [64] approximations, Hill [65] computed the shear modulus (G) for the cubic phase structure [28, 60] as express in Eq. (12)-14.

$$G_V = \frac{1}{5}(C_{11} - C_{12} + (3C_{44})) \tag{12}$$

$$G_r = \frac{5C_{44}X(C_{11} - C_{12})}{4C_{44} + 3(C_{11} - C_{12})} \tag{13}$$

$$G = \frac{G_V + G_r}{2} \tag{14}$$

The hardness of a material is indicated by its shear modulus, which quantifies its resistance to transverse deformations. A higher shear modulus suggests that the material will be harder to shape. The results for G reveal that the $Ga_{0.75}In_{0.25}As$ alloy exhibits the highest value (664.9089) at 30 GPa, followed by the doped $Ga_{0.75}Ti_{0.25}As$ sample (488.3368) at the same pressure. On the other hand, at 30 GPa, $Ga_{0.75}Sn_{0.25}As$ records the lowest G value (260.2204). Interestingly, unlike the other compounds, which typically increase with increasing pressure, the shear modulus of $Ga_{0.75}Sn_{0.25}As$ varies with pressure changes. This variation suggests that $Ga_{0.75}Sn_{0.25}As$ exhibits special

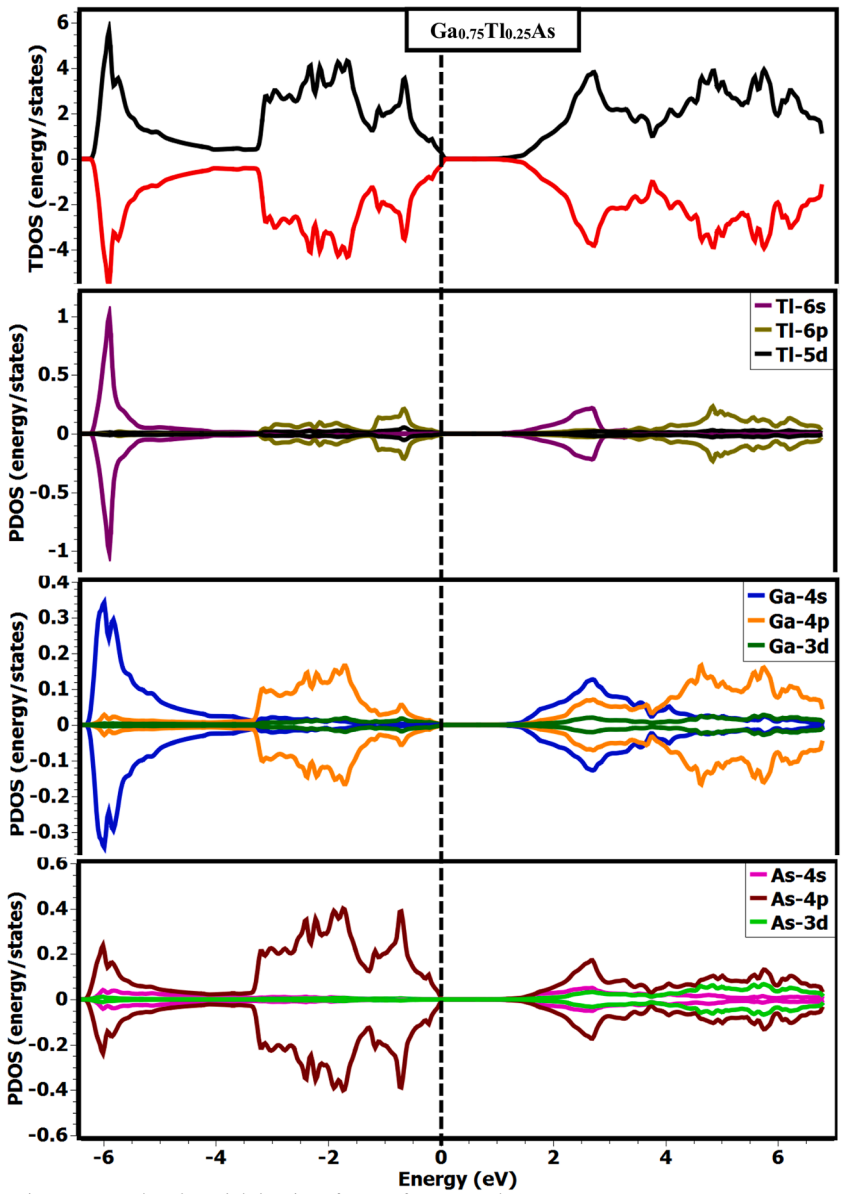

Fig. 8. Total and partial density of states for $Ga_{0.75}Tl_{0.25}As$.

behaviour under pressure. Additionally, doping seems to affect the shear modulus results, with the exception of $Ga_{0.75}Sn_{0.25}As$.

Numerous mechanical properties, such as the shear anisotropy (A), internal strain factor (PSI), Cauchy pressure (Pc), Young's modulus (Y), Poisson's ratio (V), Pugh's ratio (RP), and Frantsevich's ratio (RF), were calculated using the following equations respectively:

$$A = \frac{2C_{44}}{C_{11} - C_{12}} \tag{15}$$

$$PSI = \frac{C_{11} + 8C_{12}}{7C_{11} + 2C_{12}} \tag{16}$$

$$Y = \frac{9BG}{3B + G} \tag{17}$$

$$\nu = \frac{3B - 2G}{6B + 2G} \tag{18}$$

When the shear anisotropy (A) is 1, the material is said to be isotropic, meaning that it can deform uniformly in all directions along its body. On the other hand, a material is categorized as elastic anisotropic if the shear anisotropy deviates from unity, either more or less [66]. All of the alloys under study have calculated shear anisotropy values greater than 1, indicating that they are anisotropic. Furthermore, the results show that all anisotropy values are influenced by pressure, with higher pressure corresponding to increased anisotropy.

The Internal Strain Factor (PSI) as expressed in Eq. (16) is a measure used in materials science to gauge the magnitude of internal strains within a material. It's a quantification of the stress-related deformations or distortions present within a substance even in the absence of external forces. PSI values greater than 0.60 suggest that the material is less prone to distortion or deformation under applied stress or pressure. This means that materials with PSI values above this threshold tend to maintain their shape and resist deformation more effectively. The Internal Strain Factor (PSI) for all samples exceeds 0.60, indicating that the studied alloy materials can maintain their shape and resist deformation more effectively.

Cauchy pressure (P_C) is a mechanical parameter that determines brittleness and ductility of a studied alloy material. Eq. (17) was used to calculate P_C of the studied alloy materials, if P_C is negative the material is said to be brittle material and if it's positive, the material is said to be

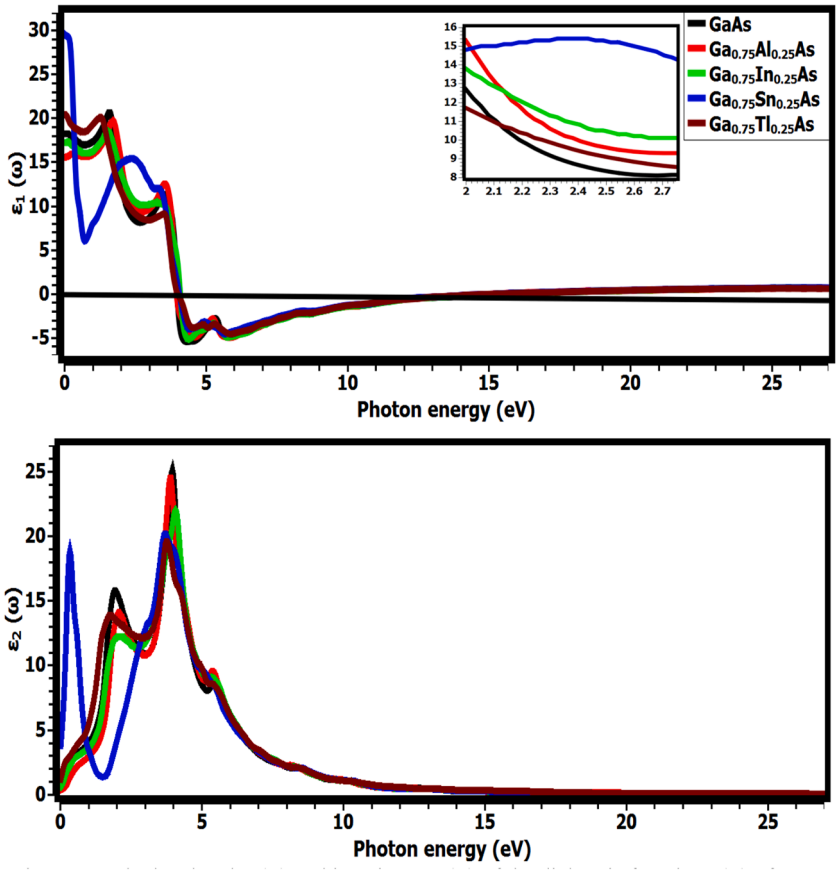

Fig. 9. Calculated real $\varepsilon_1(\omega)$ and imaginary $\varepsilon_2(\omega)$ of the dielectric function $\varepsilon(\omega)$ of GaAs and $Ga_{0.75}A_{0.25}As$ (A=Al, In, Sn and Tl) compounds.

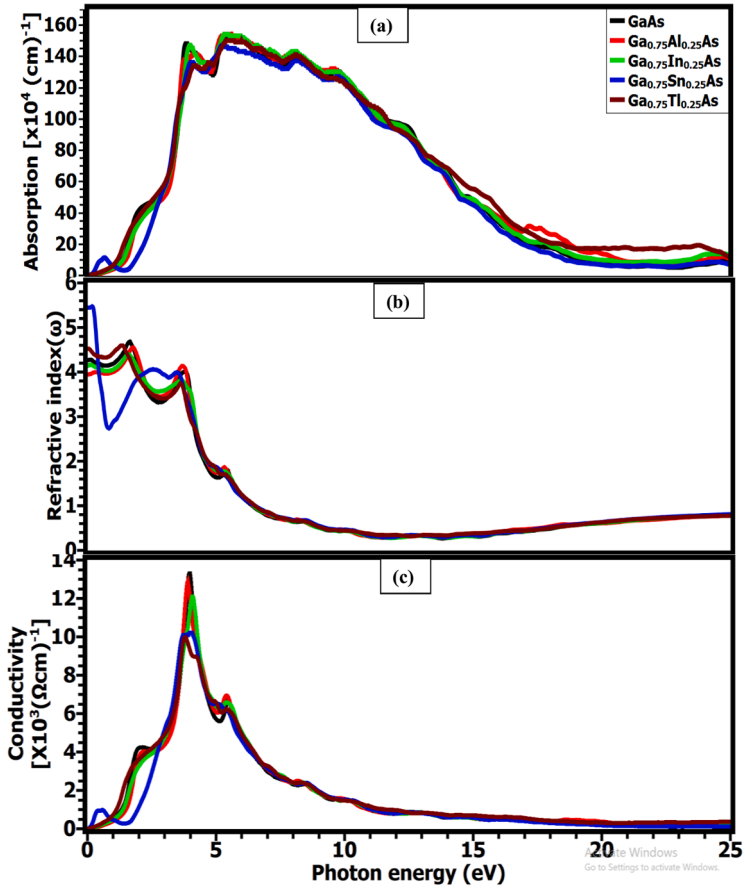

Fig. 10. Calculated absorption, refractive index and conductivity of GaAs and $Ga_{0.75}A_{0.25}As$ (A=Al, In, Sn and Tl) compounds.

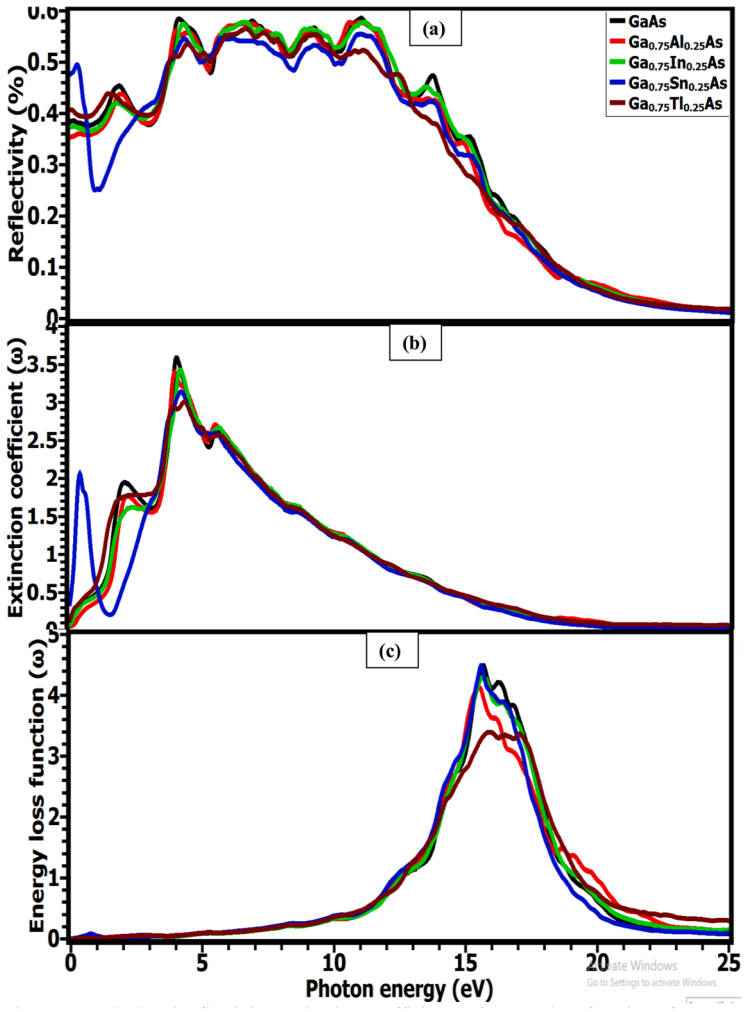

Fig. 11. Calculated reflectivity, extinction coefficient and energy loss function of GaAs and $Ga_{0.75}A_{0.25}As$ (A=Al, In, Sn and Tl) compounds.

ductile. All the studied alloy materials are result to be brittle due to their negative P_C values except $Ga_{0.75}Sn_{0.25}As$, which shows ductility under particular pressure values.

For solid materials, Poisson's ratio is an essential metric that reveals properties like brittleness or ductility, shear stability, and the nature of interatomic forces as expressed in Eq. (19) [28]. Poisson's ratio greater than 0.26 indicates ductility in materials, while values less than 0.26 indicate brittleness. Similarly, the ductility or brittleness of a material can be predicted using the Pugh's ratio (R_P), and Frantsevich's ratio (R_F) [28] which are expressed in Eq. (20 and 21) respectively. Pugh's ratio (R_P) above 1.75 denotes ductility; below 1.75, brittleness is indicated. The inverse of Pugh's ratio, Frantsevich's ratio (R_F) which indicates ductility if it is less than 0.571, it also indicates brittleness if its greater than 0.571 [28]. Based on R_P results, all the sample materials are brittle; this is because the calculated values are less than 1.75, with the exception of $Ga_{0.75}Sn_{0.25}As$, which shows ductility under particular

Table 3a
Calculated mechanical properties of pristine GaAs at different pressure.

Mechanical parameters	Values of Pressure (GPa)						
	0	5	10	15	20	25	30
C_{11}	1041.377	903.3332	929.5223	959.0582	985.0865	1009.651	1033.248
C_{12}	522.6092	397.6624	419.1128	445.2836	472.2341	492.2195	515.0378
C_{44}	697.508	603.8177	621.7464	640.261	657.7677	674.9086	691.7253
C_{11}- C_{12}	518.7675	505.6708	510.4095	513.7746	512.8524	517.4316	518.2104
P_C	−174.899	−206.155	−202.634	−194.977	−185.534	−182.689	−176.687
C_{11}+2C_{12}	2086.595	1698.658	1767.748	1849.625	1929.555	1994.09	2063.324
B	695.5317	566.2193	589.2493	616.5418	643.1849	664.6967	687.7746
G	469.2611	425.8318	435.0066	443.9192	450.8744	459.5455	466.7068
Y	1149.311	1021.435	1047.301	1073.994	1096.424	1120.429	1141.844
R_P	1.482185	1.329678	1.354576	1.388861	1.426528	1.446422	1.473676
R_F	0.67468	0.752062	0.738239	0.720015	0.701003	0.691361	0.678575
A	2.689097	2.388185	2.436265	2.492381	2.565134	2.608687	2.66967
PSI	0.626556	0.573793	0.583049	0.594601	0.607515	0.614432	0.623704
V	0.224597	0.199341	0.203775	0.209673	0.215887	0.219063	0.2233
θ_D	342.758	329.177	332.179	335.085	337.173	339.893	342.003

Table 3b
Calculated mechanical properties of doped $Ga_{0.75}Al_{0.25}As$ at different pressure.

Mechanical parameters	Values of Pressure (GPa)						
	0	5	10	15	20	25	30
C_{11}	926.8568	950.612	974.2657	997.1965	1020.303	1098.594	1058.554
C_{12}	409.1837	430.8111	453.304	475.3443	497.3847	574.9839	534.3389
C_{44}	617.8098	635.6821	652.9964	670.0052	686.8037	745.8643	715.5391
C_{11} - C_{12}	517.6731	519.8009	520.9617	521.8521	522.918	523.61	524.2156
P_C	−208.626	−204.871	−199.692	−194.661	−189.419	−170.88	−181.2
C_{11}+2C_{12}	1745.224	1812.234	1880.874	1947.885	2015.072	2248.562	2127.232
B	581.7414	604.078	626.9579	649.2951	671.6906	749.5205	709.0774
G	435.795	444.0606	451.7056	459.0738	466.3638	490.5018	478.5339
Y	1046.153	1069.996	1092.698	1114.547	1136.145	1207.993	1171.962
R_P	1.334897	1.36035	1.387979	1.414359	1.440272	1.528069	1.48177
R_F	0.749121	0.735105	0.720472	0.707034	0.694313	0.654421	0.674868
A	2.386872	2.445868	2.506888	2.567797	2.626813	2.848931	2.729942
PSI	0.574886	0.585039	0.595446	0.605209	0.614409	0.644614	0.62903
V	0.200281	0.204785	0.209524	0.213908	0.218088	0.231385	0.224534
θ_D	345.524	348.189	350.596	352.87	355.104	362.123	358.724

Table 3c
Calculated mechanical properties of doped $Ga_{0.75}Tl_{0.25}As$ at different values of pressure.

Mechanical parameters	Values of Pressure (GPa)						
	0	5	10	15	20	25	30
C_{11}	948.9241	972.7066	994.2959	1015.615	1038.687	1061.22	1083.558
C_{12}	436.271	460.0549	482.3643	504.6596	528.1975	551.0982	572.8066
C_{44}	663.4694	680.9899	698.5297	716.1103	612.9275	736.6336	752.4363
C_{11} - C_{12}	512.6531	512.6517	511.9316	510.9558	510.4897	510.1214	510.7518
P_C	−227.198	−220.935	−216.165	−211.451	−84.73	−185.535	−179.63
C_{11}+2C_{12}	1821.466	1892.816	1959.025	2024.935	2095.082	2163.416	2229.172
B	607.1554	630.9388	653.0082	674.9782	698.3607	721.1387	743.0572
G	453.1585	460.3472	467.2224	473.954	431.3113	481.842	488.3363
Y	1088.636	1110.87	1131.748	1152.183	1073.031	1182.219	1201.747
R_P	1.33983	1.370572	1.397639	1.424143	1.619157	1.496629	1.52161
R_F	0.746363	0.729623	0.715492	0.702177	0.617605	0.668168	0.657199
A	2.588375	2.656735	2.728997	2.803023	2.401331	2.888072	2.946387
PSI	0.590697	0.602033	0.612408	0.622383	0.632177	0.641212	0.648989
V	0.201165	0.206556	0.211145	0.215501	0.243917	0.22677	0.23045
θ_D	303.094	305.006	306.761	308.461	301.277	310.929	312.536

pressure conditions.

$$V = \frac{3B - 2G}{6B + 2G} \tag{19}$$

$$R_P = \frac{B}{G} \tag{20}$$

and $$R_F = \frac{G}{B} \tag{21}$$

However, considering Poisson's ratio, all studied alloys are brittle, except for the $Ga_{0.75}Sn_{0.25}As$-doped sample showing ductility at 25 GPa (0.303058) and 30 GPa (0.308685). Frantsevich's ratio further confirms brittleness in all alloys except $Ga_{0.75}Sn_{0.25}As$, which displays ductility under certain pressure conditions. Cauchy pressure, Poisson's and Pugh's ratio results are consistent with Frantsevich's ratio, which further verifies brittleness in all studied alloy materials with the exception of $Ga_{0.75}Sn_{0.25}As$, which exhibits ductility under specific pressure conditions.

An important parameter in solids, the Debye Temperature (θ_D) is correlated with thermodynamic properties such as internal vibrational energy, thermal expansion, and entropy [67]. By using mechanical properties that can be accessed via average sound velocity, it offers insights into thermodynamic behaviours [68]. Stronger covalent bonds or bond strength in materials are indicated by higher Debye temperatures [67,68]. The calculated Debye temperature increases with increased in pressure across all the three studied doped alloy materials ($Ga_{0.75}Al_{0.25}As$, $Ga_{0.75}In_{0.25}As$, and $Ga_{0.75}Ti_{0.25}As$). Interestingly, under pressure, pristine GaAs and $Ga_{0.75}Sn_{0.25}As$ exhibits a decreasing Debye temperature. The highest Debye temperature values are found in $Ga_{0.75}Al_{0.25}As$, followed by pristine GaAs, and the lowest in $Ga_{0.75}Sn_{0.25}As$. These findings imply that, in comparison to other alloys under investigation, $Ga_{0.75}Al_{0.25}As$ has stronger covalent bonds and better thermal conductivity.

4. Conclusion

The structural, electronic, optical, and mechanical properties of pristine GaAs compound and its alloy were investigated using density functional theory (DFT) ($Ga_{0.75}Al_{0.25}As$, $Ga_{0.75}In_{0.25}As$, $Ga_{0.75}Sn_{0.25}As$, $Ga_{0.75}Ti_{0.25}As$). The WIEN2K and Quantum expresso (QE) codes were used for calculations, with the generalized gradient approximation (GGA) in Perdew-Burke Erzenhoff (PBE) as the exchange correlation function for both codes. When using Standard DFT, we discovered that the band gap was underestimated, whereas DFT + mbj potential was used to correct the band gap. The semiconductor nature of pristine GaAs and its doped alloys was confirmed in this study, and the presence of Sn dopant caused the material to exhibit metallic character. The orbital contributions in the system are shown by TDOS and PDOS. Using Kramers-Kronig transformations, optical parameters such as dielectric function, absorption, refractive index, extinction coefficient, optical conductivity, and reflectivity were calculated from the dielectric constant. The performance of GaAs and some doped alloys demonstrated that the material could be used in a variety of applications, including solar cell window layer, reflection – resistant, bio-medics, and nano-optoelectronics, and lower reflectivity values can be used in the anti-reflection industry. The elastic constants and bulk modulus of the

Table 3d
Calculated mechanical properties of doped $Ga_{0.75}Sn_{0.25}As$ at different values of pressure.

Mechanical parameters	Values of Pressure (GPa)						
	0	5	10	15	20	25	30
C_{11}	678.8412	694.6557	708.1007	719.5863	732.0828	744.7522	754.1872
C_{12}	370.3831	402.8032	425.0347	447.4525	469.1485	492.1602	512.9225
C_{44}	372.9401	694.6557	393.63	403.1445	413.7823	423.3485	432.5861
C_{11} - C_{12}	308.4581	291.8525	283.066	272.1338	262.9343	252.592	241.2647
P_C	−2.55703	−291.852	31.40466	44.30794	55.36622	68.8117	80.33644
C_{11}+2C_{12}	1419.607	1500.262	1558.17	1614.491	1670.38	1729.073	1780.032
B	473.2025	500.0874	519.39	538.1638	556.7933	576.3575	593.3441
G	261.708	376.284	261.3257	261.0738	261.7217	261.3284	260.2204
Y	662.9141	902.4953	671.3782	674.1989	678.8069	681.0524	681.0932
R_P	1.808132	1.329016	1.98752	2.061347	2.127425	2.205491	2.28016
R_F	0.553057	0.752437	0.50314	0.48512	0.470052	0.453414	0.438566
A	2.418093	4.760321	2.781189	2.962841	3.14742	3.352034	3.585988
PSI	0.66305	0.691063	0.707515	0.724747	0.739793	0.755461	0.770412
V	0.266515	0.199221	0.284562	0.291204	0.296811	0.303058	0.308685
θ_D	254.437	252.763	252.595	251.763	251.317	250.384	249.022

Table 3e
Calculated mechanical properties of doped $Ga_{0.75}In_{0.25}As$ at different values of pressure.

Mechanical parameters	Values of Pressure (GPa)						
	0	5	10	15	20	25	30
C_{11}	833.258	856.0419	877.1442	897.643	920.6558	966.9121	967.8885
C_{12}	385.5222	408.163	427.0329	446.4087	468.2724	512.674	513.4191
C_{44}	559.0562	576.7438	593.9988	611.2971	628.8944	662.8691	663.175
C_{11} - C_{12}	447.7358	447.8789	450.1113	451.2343	452.3834	454.2381	454.4693
P_C	−173.534	−168.581	−166.966	−164.888	−160.622	−150.195	−149.756
C_{11}+2C_{12}	1604.302	1672.368	1731.21	1790.46	1857.201	1992.26	1994.727
B	534.7675	557.456	577.07	596.8201	619.0669	664.0867	664.9089
G	387.3153	394.707	402.5868	410.038	417.5636	431.807	432.0143
Y	935.9791	958.0136	979.8903	1000.896	1022.743	1064.663	1065.318
R_P	1.380703	1.412329	1.433405	1.455524	1.482569	1.537925	1.53909
R_F	0.724269	0.708051	0.697639	0.687038	0.674505	0.650227	0.649735
A	2.49726	2.575445	2.639342	2.709444	2.78036	2.918598	2.918459
PSI	0.593205	0.605313	0.613864	0.622731	0.632265	0.650305	0.6505
V	0.208291	0.213576	0.216993	0.220492	0.224655	0.2328	0.232966
θ_D	304.759	307.036	309.475	311.707	313.983	318.228	318.267

compound have also been predicted, with the calculated elastic constant indicating that the investigated compounds are stable and the bulk modulus of the materials indicating that doping has an effect on the bulk modulus of the materials. Cauchy pressure, Poisson's and Pugh's ratio results are consistent with Frantsevich's ratio, which verifies brittleness in all studied alloy materials with the exception of $Ga_{0.75}Sn_{0.25}As$, which exhibits ductility under specific pressure conditions. The highest Debye temperature values are found in $Ga_{0.75}Al_{0.25}As$, followed by pristine GaAs, and the lowest in $Ga_{0.75}Sn_{0.25}As$. These findings imply that, in comparison to other alloys under investigation, $Ga_{0.75}Sn_{0.25}As$ has stronger covalent bonds and better thermal conductivity.

CRediT authorship contribution statement

A.A. Adewale: Writing – original draft, Investigation. **A.A. Yahaya:** Formal analysis. **L.O. Agbolade:** Formal analysis. **O.K. Yusuff:** Data curation. **S.O. Azeez:** Formal analysis. **K.K. Babalola:** Formal analysis. **K.O. Suleman:** Data curation. **Y.K. Sanusi:** Data curation. **A. Chik:** Data curation.

Declaration of competing interest

The authors declare that they have no known competing financial interests or personal relationships that could have appeared to influence the work reported in this paper.

Data availability

Data will be made available on request.

Acknowledgements

Authors acknowledge the support by the Computational Materials Physics Laboratory, Faculty of Pure and Applied Science, Department of Pure and Applied Physics, Ladoke Akintola University of Technology, Ogbomoso, Oyo state, Nigeria.

Supplementary materials

Supplementary material associated with this article can be found, in the online version, at doi:10.1016/j.chphi.2024.100594.

References

[1] H. Arabi, A. Pourghazi, F. Ahmadian, Z. Nourbakhsh, First-principles study of structural and electronic properties of different phases of GaAs, Phys. B: Condens. Matter 373 (1) (2006) 16–22.
[2] A. Mujica, A. Rubio, A Muñoz and RJ Needs, Rev. Mod. Phys. 75 (2003) 863.
[3] F.A. Putra, E. Purwandari, B.S. Nugroho, Study of electronic properties of GaAs semiconductor using density functional theory, Comput. Exper. Res. Mater. Renew. Energy 4 (2) (2021) 94–101.
[4] J. Singleton, Band Theory and Electronic Properties of Solids, Vol. 2, Oxford University Press, 2001.
[5] S.L. Tan, W.M. Soong, M.J. Steer, S. Zhang, J.S. Ng, J.P. David, Dilute nitride GaInNAs and GaInNAsSb for solar cell applications, in: Physics, Simulation, and

Photonic Engineering of Photovoltaic Devices, Vol. 8256, International Society for Optics and Photonics, 2012, p. 82561E.
[6] J.W. Ager III, D.J. Friedman, J.F. Geisz, E.E. Haller, S.R. Kurtz, J.M. Olson, W. Shan, W Walukiewicz, Band Anticrossing in GaInNAs Alloys, Phys. Rev. Lett. 82 (1998). LBNL-42287.
[7] R. Amraoui, A. Aissat, J.P. Vilcot, D. Decoster, Frequency response optimization of PIN photodiode based on InGaAsN lattice matched to GaAs for High-Speed photodetection applications, Opt. Laser Technol. 145 (2022) 107468.
[8] A.A. Adewale, A. Chik, O.K. Yusuff, S.A. Ayinde, Y.K. Sanusi, First principle calculation of structural, electronic and optical properties of CdS and doped $Cd_{x-1}A_xS$ (A= Co, Fe, Ni) compounds, Mater. Today Commun. 26 (2021) 101882.
[9] P. Kusch, S. Breuer, M. Ramsteiner, L. Geelhaar, H. Riechert, S. Reich, Band gap of wurtzite GaAs: a resonant Raman study, Phys. Rev. B 86 (7) (2012) 075317.
[10] F. Yao, M. Yang, Y. Chen, X. Zhou, L. Wang, First-principles calculations of the electronic, and optical properties of a GaAs/AlAs van der Waals heterostructure, Chem. Phys. Lett. 765 (2021) 138194.
[11] H.C. Chen, C.C. Lin, H.V. Han, K.J. Chen, Y.L. Tsai, Y.A. Chang, M.H. Shih, H. C. Kuo, P. Yu, Enhancement of power conversion efficiency in GaAs solar cells with dual-layer quantum dots using flexible PDMS film, Solar Energy Mater. Solar Cell. 104 (2012) 92–96.
[12] E.M. Pavelescu, N. Bălţăţeanu, S.I. Spânulescu, E. Arola, Very high dose electron irradiation effects on photoluminescence from GaInNAs/GaAs quantum wells grown by molecular beam epitaxy, Opt. Mater. (Amst.) 64 (2017) 361–365.
[13] Mal, I., Jayarubi, J., Das, S., Sharma, A.S., Peter, A.J., & Samajdar, D.P. (2019). Hydrostatic pressure dependent optoelectronic properties of InGaAsN/GaAs spherical quantum dots for laser diode applications. Physica Status Solid. (b), 256 (3), 1800395.
[14] A. Aissat, R. Bestam, B. Alshehri, J.P. Vilcot, Modeling of the absorption properties of $Ga_{1-x}In_xAs_{1-y}N_y$/GaAs quantum well structures for photodetection applications, Superlatt. Microstruct. 82 (2015) 623–629.
[15] A. Kosa, L. Stuchlikova, L. Harmatha, M. Mikolasek, J. Kovac, B. Sciana, W. Dawidowski, D. Radziewicz, M Tlaczala, Defect distribution in InGaAsN/GaAs multilayer solar cells, Sol. Energy 132 (2016) 587–590.
[16] V. Alberts, J.H. Neethling, A.W. Leitch, Correlation between structural, optical, and electrical properties of GaAs grown on (001) Si, J. Appl. Phys. 75 (11) (1994) 7258–7265.
[17] U. Chakma, A. Kumer, K.B. Chakma, M.T. Islam, D. Howlader, R.M. Mohamed, Electronics structure and optical properties of $SrPbO_3$ and $SrPb_{0.94}Fe_{0.06}O_3$: a first principle approach, Eurasian Chem. Commun. 2 (5) (2020) 573–580.
[18] A.K. Singh, D. Chandra, S. Kattayat, S. Kumar, P.A. Alvi, A. Rathi, First-principles investigation of electronic properties of $GaAs_xSb_{1-x}$ ternary alloys, Semiconductors 53 (13) (2019) 1731–1739.
[19] M.I. Ziane, Z. Bensaad, B. Labdelli, H. Bennacer, First-principles study of structural, electronic and optical properties of III-arsenide binary GaAs and InAs, and III-nitrides binary GaN and InN: improved density-functional-theory Study, Sens. Transduc. 27 (5) (2014) 374.
[20] Blaha, P., Schwarz, K., Madsen, G.K., Kvasnicka, D., & Luitz, J. (2001). wien2k. An augmented plane wave+ local orbitals program for calculating crystal properties, 60.
[21] J.P. Perdew, K. Burke, M. Ernzerhof, Perdew, burke, and ernzerhof reply, Phys. Rev. Lett. 80 (4) (1998) 891.
[22] P. Hohenberg, W. Kohn, Inhomogeneous electron gas, Phys. Rev. 136 (3B) (1964) B864.
[23] F. Tran, P. Blaha, Accurate band gaps of semiconductors and insulators with a semilocal exchange-correlation potential, Phys. Rev. Lett. 102 (22) (2009) 226401.
[24] S. Khatta, V. Kaur, S.K. Tripathi, S. Prakash, The first principles study of elastic and thermodynamic properties of ZnSe, in: AIP Conference Proceedings 1953, AIP Publishing LLC, 2018 130016.
[25] P. Giannozzi, S. Baroni, N. Bonini, M. Calandra, R. Car, C. Cavazzoni, D. Ceresoli, G.L. Chiarotti, M. Cococcioni, R.M Dabo Wentzcovitch, QUANTUM ESPRESSO: a modular and open-source software project for quantum simulations of materials, J. Phys.: Conden. Matter 21 (39) (2009) 395502.
[26] D.D. Koelling, B.N. Harmon, A technique for relativistic spin-polarised calculations, J. Phys. C: Solid State Phys. 10 (16) (1977) 3107.
[27] H.J. Monkhorst, J.D. Pack, Special points for Brillouin-zone integrations, Phys. Rev. B 13 (12) (1976) 5188.
[28] A.A. Adewale, A. Chik, T. Adam, O.K. Yusuff, S.A. Ayinde, Y.K. Sanusi, First principles calculations of structural, electronic, mechanical and thermoelectric properties of cubic $ATiO_3$ (A= Be, Mg, Ca, Sr and Ba) perovskite oxide, Comput. Conden. Matter 28 (2021) e00562.
[29] C. Ambrosch-Draxl, J.O. Sofo, Linear optical properties of solids within the full-potential linearized augmented planewave method, Comput. Phys. Commun. 175 (1) (2006) 1–14.
[30] T.V. Vu, K.D. Pham, T.N. Pham, D.D. Vo, P.T. Dang, C.V. Nguyen, H.V. Phuc, N. T. Binh, D.M. Hoat, N.N. Hieu, First-principles prediction of chemically functionalized InN monolayers: electronic and optical properties, RSC Adv. 10 (18) (2020) 10731–10739.
[31] M. Rizwan, S. Aleena, M. Shakil, T. Mahmood, A.A. Zafar, T. Hussain, M.H. Farooq, A computational insight of electronic and optical properties of Cd-doped $BaZrO_3$, Chin. J. Phys. (2020).
[32] A.A. Adewale, A. Chik, T. Adam, T.M. Joshua, M.O. Durowoju, Optoelectronic behavior of ZnS compound and its alloy: a first principle approach, Mater. Today Commun. 27 (2021) 102077.
[33] M.I. Ziane, Z. Bensaad, T. Ouahrani, B. Labdelli, H.B. Nacer, H. Abid, First-principles prediction of the structural and electronic properties of zinc blende GaN_xAs_{1-x} alloys, Mater. Sci. Semicond. Process. 16 (4) (2013) 1138–1147.
[34] F.E.H. Hassan, A.V. Postnikov, O. Pagès, Structural, electronic, optical and thermal properties of $Al_xGa_{1-x}AsySb_{1-y}$ quaternary alloys: first-principles study, J. Alloy. Compd. 504 (2) (2010) 559–565.
[35] S. Adachi, Band gaps and refractive indices of AlGaAsSb, GaInAsSb, and InPAsSb: key properties for a variety of the 2–4-μm optoelectronic device applications, J. Appl. Phys. 61 (10) (1987) 4869–4876.
[36] M.H. Hachemi, M. Benchehima, K. Bencherif, H. Abid, The effect of N-incorporation on the structural and optoelectronic properties of GaP and GaAs for optical telecommunication applications: first-principles study, Optik (Stuttg) (2022) 169282.
[37] K.H. Hellwege, O. Madelung, L. Bornstein, Semiconductors physics of group IV elements and III–V alloys, New Series Group III (1982) 17.
[38] S.N. Ahmed, Physics and Engineering of Radiation Detection, 2nd edition, Academic Press, 2015.
[39] J. Li, X. Han, C. Dong, C. Fan, Theoretical investigation of structural, mechanical and electronic properties of $GaAs_{1-x}N_x$ alloys under ambient and high pressure, Physica B: Conden. Matter 526 (2017) 1–6.
[40] R. Ahmed, S.J. Hashemifar, H. Akbarzadeh, M. Ahmed, Ab initio study of structural and electronic properties of III-arsenide binary compounds, Comput. Mater. Sci. 39 (3) (2007) 580–586.
[41] J.W. Haus, Fundamentals and Applications of Nanophotonics, Woodhead Publishing, 2016.
[42] H.H. Hegazy, M. Manzoor, M.W. Iqbal, M. Zanib, A. Dahshan, I. Kebaili, Systemically study of optoelectronic and transport properties of chalcopyrite $HgAl_2X_4$ (X= S, Se) compounds for solar cell device applications, J. Mater. Res. Technol. 19 (2022) 1690–1698.
[43] Othman, M.S., & Elkenany, E.B. (2022). Structural and optical properties of GaAs and InAs for doping Sb under the effect of pressure and temperature: DFT and EPM investigations.
[44] L. Salasnich, Quantum Physics of Light and Matter, Springer International PU, 2017.
[45] L. Yu, D. Li, S. Zhao, G. Li, K. Yang, First principles study on electronic structure and optical properties of ternary GaAs: bi alloy, Mater. (Basel) 5 (12) (2012) 2486–2497.
[46] M.A. Khan, H. Algarni, N. Bouarissa, Temperature dependence of the optical and lattice vibration properties in gallium arsenide, Optik (Stuttg) 176 (2019) 366–371.
[47] M.J.I. Khan, Z. Kanwal, M.N. Usmani, M. Yousef, P. Akhtar, A. Nabi, Effect of Ni concentration on optical properties of rocksalt CdS system (A DFT+ U study), Int. J. Mod. Phys. B 32 (25) (2018) 1850280.
[48] H. Umm, G. Murtaza, H.R. Hafiz, Optoelectronic and thermal properties of cubic $SiMO_3$ (M = Sn, Pb) oxides for device application: a first principle study". Optical and Quantum Electronics, 2020.
[49] A. Laref, A. Altujar, S. Laref, S.J. Luo, Quantum confinement effect on the electronic and optical features of InGaN-based solar cells with InGaN/GaN superlattices as the absorption layers, Sol. Energy 142 (2017) 231–242.
[50] Prangnell, L. (2016). Visible Light-Based Human Visual System Conceptual Model. arXiv preprint arXiv:1609.04830.
[51] D. Ma, Y. Cao, J. Zhang, Y. Deng, W. Wang, E. Li, Density functional theory study on the properties of Cu-doped GaAs, Vacuum 175 (2020) 109252.
[52] P.D.C. King, T.D. Veal, C.E. Kendrick, L.R. Bailey, S.M. Durbin, C.F. McConville, InN/GaN valence band offset: high-resolution x-ray photoemission spectroscopy measurements, Phys. Rev. B 78 (3) (2008) 033308.
[53] A. Janotti, B. Jalan, S. Stemmer, C.G. Van de Walle, Effects of doping on the lattice parameter of $SrTiO_3$, Appl. Phys. Lett. 100 (26) (2012) 262104.
[54] M.K. Rabadanov, A harmonic temperature factors and charge density in ZnS, Cry. Rp. 40 (1) (1995) 17–22.
[55] A.A. Sholagberu, W.A. Yahya, A.A. Adewale, Pressure effects on the opto-electronic and mechanical properties of the double perovskite $Cs_2AgInCl_6$, Phys. Scr. 97 (2022) 085824.
[56] S.A. Dar, V. Srivastava, U. Kumar, U.K. Sakalle, A. Vanshree, V. Parey, Electronic structure, magnetic, mechanical and thermophysical behavior of double perovskite Ba_2MgO_6, Eur. Phys. J. Plus 133 (2018) 64.
[57] M. Born, K. Huang, M. Lax, Electronic structure, magnetic, Am. J. Phys. 23 (1955) 474.
[58] N. Dharmale, S. Chaudhury, R. Mahamune, D. Dash, Comparative study on structural, electronic, optical and mechanical properties of normal and high pressure phases titanium dioxide using DFT, Mater. Res. Expr. 7 (2020) 054004, https://doi.org/10.1088/2053-1591/ab8d5c, 2020.
[59] M.H. Elahmar, H. Rached, D. Rached, S. Benalia, R. Khenata, Z.E. Biskri, S. B. Omran, Structural stability, electronic structure and magnetic properties of the new hypothetical half-metallic ferromagnetic full-Heusler alloy CoNiMnSi, Mater. Sci.-Poland 34 (1) (2016) 85–93.
[60] W.A. Yahya, A.A. Yahaya, A.A. Adewale, A.A. Sholagberu, N.K. Olasunkanmi, A dft study of optoelectronic, elastic and thermoelectric properties of the double perovskites Rb_2SeX_6(X=Br,Cl), J. Nig. Soc. Phys. Sci. 5 (2023) 1418.
[61] S. Tariq, A. Ahmed, S. Saad, S. Tariq, Structural, elastic and elastic properties of the cubic $CaTiO_3$ under pressure: a DFT study, AIP Adv. 5 (7) (2015) 077111, 2015.
[62] A. Reuß, Berechnung der fließgrenze von mischkristallen auf grund der plastizitätsbedingung für einkristalle, ZAMM-J. Appl. Math. Mech./Zeitschrift für Angewandte Mathematik und Mechanik 9 (1) (1929) 49–58, 1929.
[63] R. Hill, The elastic behaviour of a crystalline aggregate, Proc. Phys. Soc. 65 (5) (1952) 349, 1952.
[64] Nye, J.N. (1985). Physical Properties of Crystals Their Representation by Tensors and Matrices. Number ISBN:9780198511656. illus.

[65] T. Jinzhong, Z. Yuhong, H. Hua, W. Bing, The effect of alloying elements on the structural stability, mechanical properties, and Debye temperature of Al_3Li: a first-principles study, Mater. (Basel) 11 (2018) 1471, https://doi.org/10.3390/ma11081471. www.mdpi.com/journal/materials.

[66] W. Qing, J. Peng, X. Wang, First principles investigation of pressure dependent stability, phonon, Debye temperature, physical, mechanical and thermodynamic properties of Rh_3Al intermetallic compound, Mol. Simul. (2018), https://doi.org/10.1080/08927022.2018.1521969.

[67] J. Tian, Y. Zhao, H. Hou, B. Wang, The effect of alloying elements on the structural stability, mechanical properties, and Debye temperature of Al_3Li: a first-principles study, Materials 11 (8) (2018) 1471.

[68] W. Qing, J. Peng, X. Wang, First principles investigation of pressure dependent stability, phonon, Debye temperature, physical, mechanical and thermodynamic properties of Rh_3Al intermetallic compound, Mol. Simul. 44 (18) (2018) 1554–1563.